Moisture and Precipitation Evolution during Tropical Cyclone Formation as Revealed by the SSM/I–SSMIS Retrievals

ZHUO WANG

Department of Atmospheric Sciences, University of Illinois at Urbana–Champaign, Urbana, Illinois

ISAAC HANKES

Department of Geography, Northern Illinois University, DeKalb, Illinois

(Manuscript received 9 October 2015, in final form 9 April 2016)

ABSTRACT

The simultaneous precipitation and column water vapor retrievals from the SSM/I and SSMIS passive microwave instruments were used to examine the convective and moisture evolution during tropical cyclone formation. Using a wave-pouch-track dataset, composites of precipitation and column water vapor were constructed with more than 2000 satellite overpasses for a 3-day time period prior to genesis. It was found that high column water vapor occurs near the pouch center and starts to increase about 42 h prior to genesis while a substantial increase in precipitation occurs within 24 h prior to genesis. These features are consistent with a recently proposed two-stage conceptual model for tropical cyclone formation, in which gradual moisture preconditioning precedes an abrupt transition to sustained deep convection leading up to genesis.

The relationship between precipitation and saturation fraction (SF) is examined for the developing waves and compared with the general tropical North Atlantic. Precipitation rate is found to increase at the same exponential rate above the same critical point of SF in the two groups, but convection in the developing waves has a higher probability of occurrence near and above criticality. This can be attributed to the positive feedback between convection and the low-level moisture convergence, which counteracts the negative feedback of convection on water vapor and makes convection in a developing tropical cyclone more sustainable.

1. Introduction

As a vigorous rotating system, tropical cyclones (TCs) are characterized by circularly organized deep convection in a relatively small region, which is in sharp contrast to transient, scattered convection in ordinary tropical convective systems or broadly organized convection in open equatorial waves. Latent heat release of the tightly organized convection near the storm center drives the transverse circulation, and the associated low-level inflow converges moisture from the warm ocean at large radii fueling further precipitation (Fritz and Wang 2014) and intensifying the system-scale circulation (Tory and Frank 2010; Wang et al. 2010a; Montgomery and Smith 2010; Fang and Zhang 2010; Raymond and López Carrillo 2011). TC formation can thus be regarded as a process in which convection becomes stronger and better organized in a tight, quasi-circular pattern (Wang 2014). To investigate the key mechanisms for convective organization, it is necessary to document the convective evolution leading up to genesis.

Zehr (1992) provided one of the first detailed reports on the convective evolution during tropical cyclogenesis using satellite data. He tracked 50 storms over the western North Pacific during 1983 and 1984 and proposed a two-phase conceptual model for TC formation. The first phase is characterized by a convective maximum that initiates a mesoscale vortex; the second phase is marked by increasing deep convection associated with the low-level circulation center. However, as the author pointed out, the convective maximum in phase one is highly variable in the intensity and extent of deep convection and does not distinguish a developer from a nondeveloper. It is also worth noting that TC genesis in Zehr (1992) is defined as the formation of a tropical storm. The time interval between the early convective maximum (in phase 1) and genesis varies

Corresponding author address: Zhuo Wang, Department of Atmospheric Sciences, University of Illinois at Urbana–Champaign, 105 South Gregory St., Urbana, IL 61801.
E-mail: zhuowang@illinois.edu

DOI: 10.1175/JAS-D-15-0306.1

from less than 1 day to more than 8 days among individual cases, and a tropical depression may form in the first phase or the second phase. Lee et al. (2008) examined the evolution of mesoscale features during tropical cyclone formation for different types of synoptic-scale environments over the western North Pacific. They focused on a 2-day time window prior to genesis and found storms with different patterns of pregenesis convective evolution. In addition to storms with two convective peaks that fit the conceptual model by Zehr (1992), they also identified other scenarios, including storms with one convective peak, with three convective peaks, with gradually deepening convection, or with highly fluctuating convection. The various scenarios indicate the impacts of the synoptic-scale flow on the mesoscale convection and the complex nature of tropical cyclogenesis.

High-resolution numerical model simulations and field observations have also been used to investigate the convective and thermodynamic evolution during tropical cyclogenesis. Using idealized simulations, Nolan (2007) showed that a nearly saturated inner core leads to the rapid development of a tropical cyclone. The analyses of dropsonde data from the PREDICT field experiment by Wang (2012) showed that the midlevel equivalent potential temperature θ_e increases significantly 1–2 days prior to genesis at the inner-pouch[1] region but changes little at the outer region. Davis and Ahijevych (2013) also showed that the moist static energy increases in the middle troposphere prior to genesis. The increase in θ_e is due to the midlevel moistening, and the high column moisture content near the pouch center is owing to the dynamic and kinematic structure of the wave pouch (Wang 2012). The differential moistening between the inner- and outer-pouch regions was also demonstrated in a numerical model simulation (Wang 2012) and through the diagnoses of the ERA-Interim data (Wang and Hankes 2014). A follow-up study by Wang (2014) showed that the transition to sustained deep convection occurs after column moistening near the pouch center and that the transition is marked by a substantial increase in precipitation and the rapid vertical development of the protovortex within 24 h prior to genesis.

The objective of the study is to document the moisture and precipitation evolution in tropical cyclogenesis using the Special Sensor Microwave Imager (SSM/I) and the Special Sensor Microwave Imager/Sounder (SSMIS) data. A particular strength of the dataset is the simultaneous retrievals of precipitation and column water vapor (CWV). The datasets are described in section 2, and the results are presented in section 3, followed by a summary in section 4.

2. Data

a. SSM/I and SSMIS

SSM/I and SSMIS are multichannel, linearly polarized passive microwave radiometers. The instruments measure surface–atmosphere microwave brightness temperature at different frequencies, which allow the simultaneous retrievals of surface wind speed, CWV, cloud liquid water, and rain rate over the global oceans. The multisatellite dataset from Remote Sensing Systems is a product of more than 20 yr of refinements, improvements, and verifications (Wentz 2013). The CWV retrievals take the advantage of the strong water vapor absorption line near 22 GHz, in the microwave range. Owing to the high signal-to-noise ratio, the CWV measurement is very accurate, and the measurements from different satellites at the same location often agree with each other within a few tenths of a millimeter (http://www.remss.com/measurements/atmospheric-water-vapor). The daily or monthly mean data have been utilized in previous studies to examine the relationship between CWV and precipitation over tropical oceans (e.g., Bretherton et al. 2004). Here we use the version-7 daily precipitation and CWV data from all available SSM/I (i.e., f08, f10, f11, f13, f14, and f15) and SSMIS (f16 and f17) instruments during 1989–2010.[2] The orbital data were mapped to a 0.25° × 0.25° grid mesh with gaps between overpasses, and moisture retrievals subject to rain contamination are set as the missing data. The daily observations consist of two measurements: one from the ascending orbits (from south to north) and the other from the descending orbits (from north to south), which overlap in many locations. We take the advantage of the time stamp information of the ascending and descending passes of the near-polar orbiting satellites and examine the moisture and precipitation evolution on the subdaily time scale by constructing composites with respect to the genesis time [similar to the composite approaches in Mapes et al. (2009) and Masunaga (2012)]. Although continuous observations of individual storms are not available from SSM/I and SSMIS, composites provide

[1] A wave pouch is a region of quasi-closed Lagrangian circulation within the critical layer of a tropical wave (Dunkerton et al. 2009), and the pouch center is the preferred location for tropical cyclogenesis (e.g., Wang et al. 2009; Montgomery et al. 2010). The inner-pouch region is referred to as a meso-β-scale area around the pouch center.

[2] Different instruments cover different time periods, and f18 was not available at the time of this study. More information can be found at http://www.remss.com/missions/ssmi.

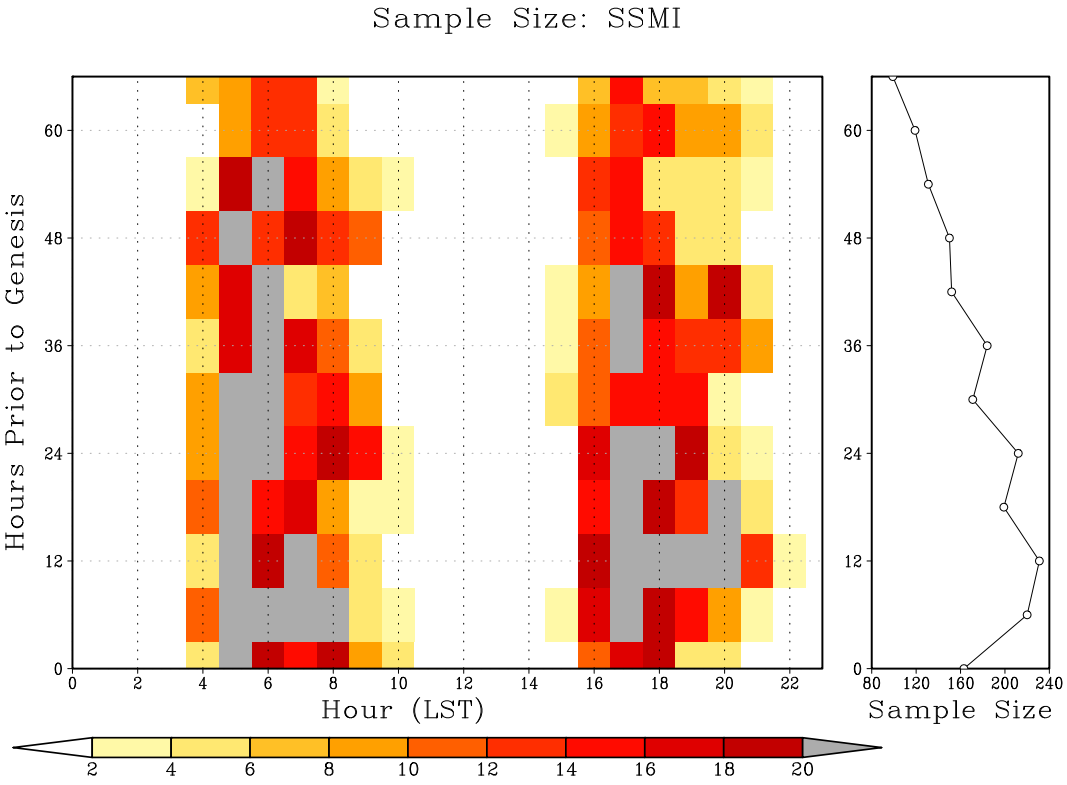

FIG. 1. (left) Number of satellite overpasses as a function of the local time at different hours prior to genesis. (right) Number of satellite overpasses as a function of hours prior to genesis. The ordinate axes indicate hours prior to genesis.

a picture of the statistically continuous evolution as shown in section 3.

b. *Saturation fraction*

In addition to CWV, we also examined saturation fraction. Saturation fraction (SF), or the column relative humidity, is defined as the ratio of the column water vapor to the saturation column water vapor from 1000 to 150 hPa. The saturation CWV is a function of tropospheric temperature and is derived from the 6-hourly temperature data from ERA-Interim. The time stamp information from the SSM/I–SSMIS overpasses is used to match them with the 6-hourly reanalysis data, and saturation fraction is calculated as the ratio of the two.

c. *A wave-pouch-track dataset*

A pouch-track dataset was constructed by Wang and Hankes (2014) using the ERA-Interim data. Here we use the 700-hPa pouch tracks and focus on the time period from 3 days prior to genesis to the genesis time. The genesis time in this study is defined as the beginning of a TC track in the best-track dataset, which, in most cases, is the formation of a tropical depression. The dataset contains more than 200 named Atlantic storms originating from tropical easterly waves during 1989–2010. After excluding storms that have a nonnegligible meridional propagation speed, 164 storms were left. The hourly pouch tracks were derived from the 6-hourly pouch tracks using the linear interpolation, and the SSM/I–SSMIS data within a 5° radius of a pouch center were then extracted to construct composites. To ensure the robustness of the results, we excluded overpasses with an areal coverage less than 25% within a 2° radius of the pouch center.

3. Results

The sample size is first examined to check whether it is large enough to construct meaningful statistics. Figure 1a shows the number of the SSM/I and SSMIS overpasses as a function of the local standard time (LST) at different hours prior to genesis. There are two clusters of measurement times: one around 0600 LST and the other around 1800 LST. Despite the gap between, a large number of observations are available throughout the 3-day time period prior to genesis, and composites of statistically continuous temporal evolution can thus be constructed. Figure 1a also shows that the observations

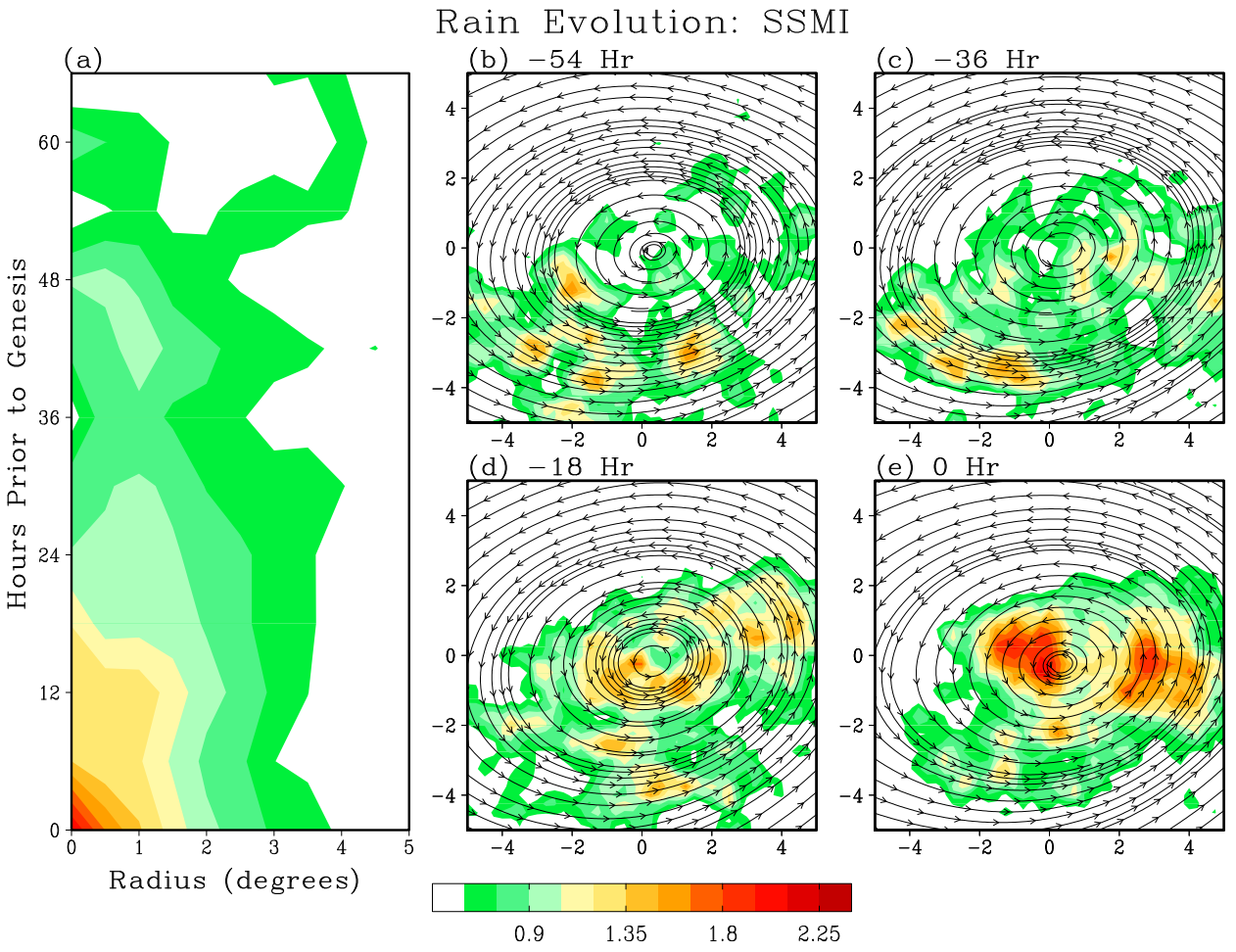

FIG. 2. (a) Radius–time plot of rain rate. (b)–(e) 2D composites of rain rate at −54, −36, −18, and 0 h, respectively, superimposed on 700-hPa streamlines. Rain rate is in millimeters per hour.

are nearly equally distributed between the two clusters (morning vs afternoon), and we can therefore assume that the diurnal variability is largely smoothed out when averaging over the two clusters. The sample size has a decreasing trend as tracking backward in time because a wave pouch is absent or located over land in some storms at the earlier times. Figure 1b shows that the number of satellite overpasses over a 6-h time interval (except that a 3-h interval was applied from −3 to 0 h) varies between ~100 and ~230. Note that one storm may get more than one overpass from the multiple instruments. The total number of satellite overpasses is 2031 from −66 to 0 h.

The time–radius plot of precipitation is shown in Fig. 2a. The plot is constructed by taking the 6-h average of azimuthal-mean precipitation centered at −66, −60, . . . , and −6 h, and a 3-h average is taken from −3 to 0 h to represent the genesis time (−72 h is not shown owing to the small sample size from −72 to −69 h). Precipitation is weak and scattered in the radial direction prior to −48 h and appears to organize from −48 h onward. The maximum precipitation occurs off the pouch center from −48 to −30 h and moves to the pouch center after −24 h (Wang et al. 2010b; Davis and Ahijevych 2012). Precipitation increases substantially from −24 h onward, especially within 6 h prior to genesis. The mean precipitation rate near the pouch center increases from ~1.0 to ~2.0 mm h^{-1} within 24 h prior to genesis. The precipitation increase is evident within 1.5° from the pouch center but is masked out by fluctuations at radii greater than 2°.

More detailed evolution of precipitation is shown in Figs. 2b–e. Superimposed on precipitation are the composite-mean translated streamlines, and the composite-mean wave pouch is indicated by the quasi-closed circulation. At −54 and −36 h, the maximum precipitation occurs south of the pouch center, and precipitation in the northern half of the wave pouch is much weaker. This is

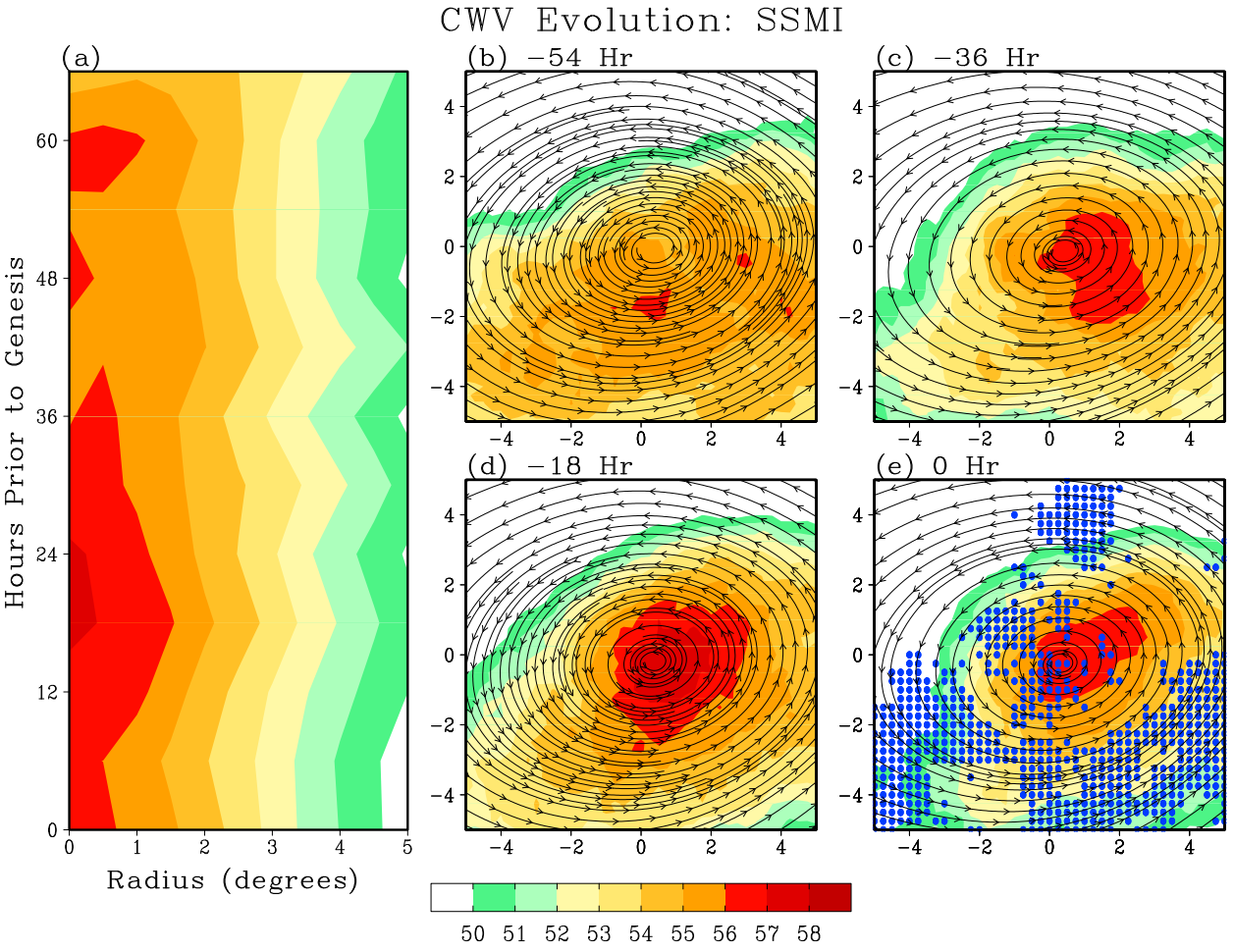

FIG. 3. (a) Radius–time plot of CWV (mm). (b)–(e) 2D composites of CWV at −54, −36, −18, and 0 h, respectively, superimposed on 700-hPa streamlines. Blue dots in (e) indicate grid points at which the decrease in CWV from −18 to 0 h exceeds the 95% confidence level.

likely due to the ITCZ, which is located south of the wave track and serves as a moisture reservoir for a developing wave. In addition, dry air in the north (see Fig. 3) may hinder convection. Maximum precipitation has moved close to the pouch center by −18 h (Fig. 2d), and the azimuthal distribution becomes more symmetric within a 2° radius. Precipitation becomes much stronger at the genesis time. It is also interesting to note that two precipitation maxima occur west and east of the pouch center instead of right at the pouch center.

The sharp increase in precipitation prior to genesis is consistent with the second stage of development in the two-stage conceptual model proposed by Wang (2014), which is characterized by an abrupt transition to sustained deep convection after the gradual low-level spinup and moisture preconditioning by cumulus congestus at the first stage. In contrast, Zehr (1992) emphasized the importance of two convective bursts. Since the two convective bursts in Zehr's conceptual model occur at various time intervals with respect to the formation of a tropical depression, they may be smoothed out or weakened when averaged over a large number of storms. In addition, a convective burst may occur more than 3 days prior to genesis and is thus not captured by Fig. 2. Therefore, Fig. 2 does not prove or disprove the conceptual model by Zehr (1992). On the other hand, one may ponder the significance of one or two short-lived convective bursts to TC formation over the course of the several-day pregenesis evolution. Wang (2014) suggested that the accumulated contribution of cumulus congestus to the low-level spinup is greater than that of sporadic deep convection although deep convection is necessary for the development of a tropospheric-deep vortex.

The column moisture evolution is shown in Fig. 3. The time–radius plot shows that CWV increases with decreasing radius, suggesting that the inner-pouch region effectively retains moisture lofted by convection and is

well protected from lateral dry-air intrusion. There are some fluctuations in CWV at the inner-pouch region in the early part of the evolution, and a seemingly robust increase starts at −42 h. In contrast, CWV does not show a clear trend at the outer-pouch region throughout the time period of analysis. The different moisture evolution between the inner- and outer-pouch regions is consistent with the dropsonde analysis by Wang (2012). Unexpectedly, CWV peaks at −18 h and then decreases from −18 to −6 h.

The 2D distribution of CWV is shown in Figs. 3b–d. At −54 h, the maximum CWV occurs south of the pouch center, and the northern half of the wave pouch is much drier than the southern half, indicating the impacts of the Saharan air layer or midlatitude dry-air intrusion (e.g., Braun 2010; Dunion 2011; Hankes et al. 2015). Moisture distribution becomes more symmetric at −36 h with the highest CWV located around the pouch center (Fig. 3c). CWV continues to increase near the pouch center by −18 h (Fig. 3d), and high CWV (>56 mm) is nearly symmetrically distributed around the pouch center, while the northwest quadrant remains relatively dry at the outer-pouch region. Intriguingly, CWV at 0 h is lower than that at −18 h in many regions, which is consistent with the decrease in CWV after −18 h shown in Fig. 3a. Since the decrease in CWV occurs extensively within the wave pouch instead of being confined to the heavily precipitating region near the pouch center, it cannot be simply attributed to the larger number of missing CWV retrievals owing to rain contamination at the genesis time. A one-tailed Student's *t* test shows that the decrease in CWV exceeds the 95% confidence level in most part of the southern pouch region.

Previous studies (Raymond 2000; Bretherton et al. 2004; Neelin et al. 2009; Peters et al. 2009) have shown that precipitation increases exponentially with CWV after CWV exceeds a critical value, which explains the rapid increase in precipitation following the increase in CWV. It has also been shown that the critical value of CWV depends on the tropospheric temperature and that a tighter relationship exists between precipitation rate and SF. To check whether the decrease in CWV from −18 to −6 h is due to temperature variations near genesis, we examined the temporal evolution of SF, which shows a similar peak at −18 h followed by a decrease (not shown).

This leads to the question whether the relationship between precipitation and tropospheric moisture in a developing tropical cyclone is the same as that over the general tropical oceans. Figure 4a shows the ensemble-mean precipitation rate stratified by column water vapor for the wave pouches. The ensemble-mean precipitation is calculated by averaging precipitation in 1-mm bins of CWV. For comparison, we also derived the ensemble-average precipitation over the tropical North Atlantic (5°–20°N, 15°–100°W), including both TCs and ordinary tropical precipitating systems. To increase the robustness of the results, the precipitation and moisture data were coarsened to a grid with 2° × 2° resolution before constructing the ensemble average. Both ensemble curves show a rapid increase in precipitation rate with increasing CWV, but large discrepancies exist for CWV > 50 mm, with the pouch curve showing a higher precipitation rate for a given CWV. A much better agreement is found between the ensemble curves when precipitation is stratified by saturation fraction (Fig. 4b). Precipitation in the two ensemble groups increases at the same exponential rate above the same critical value of SF (~80%). This suggests that the higher precipitation rate associated with the pouches shown in Fig. 4a occurs with higher saturation CWV or higher tropospheric temperature.

What is strikingly different between the two ensemble groups is the frequency of occurrence or the probability distribution function (PDF) of SF as shown in the histograms. While the histograms of CWV and SF for the tropical North Atlantic have a broad peak, the histograms for the developing waves have a much narrower distribution with a more prominent peak skewed toward high values, indicating the wave pouches are in a much moister condition. It is worth noting that the peak in the PDF and the sharp drop above criticality occur at higher values of SF in the pouch ensemble than in the tropical North Atlantic ensemble despite the same critical point. It suggests that convection spends a much larger fraction of its time near and above criticality in the pouch ensemble. The theory proposed by Neelin et al. (2009) helps to understand the similarities and differences between the two ensembles. The criticality and the exponential precipitation pickup are universal properties of convection and are thus the same for incipient TCs and ordinary tropical convection. The sharp drop in the PDF near criticality in the tropical North Atlantic ensemble is due to the negative feedback of precipitation (the order parameter) on water vapor (the tuning parameter). The higher PDF near and above criticality in the pouch ensemble can be explained by the strong interaction between convection and the atmospheric circulation. More specifically, convection enhances the low-level moisture convergence, which counteracts the negative feedback of precipitation on water vapor and makes convection sustainable. A tropical cyclone with persistent deep convection is likely in a quasi-equilibrium state with high rain rate and moderately high SF (or CWV).

Interestingly, the pouch curve in Fig. 4b shows a dip around SF = 95% and SF = 99%. The fluctuations are associated with a limited sample size for the ensemble

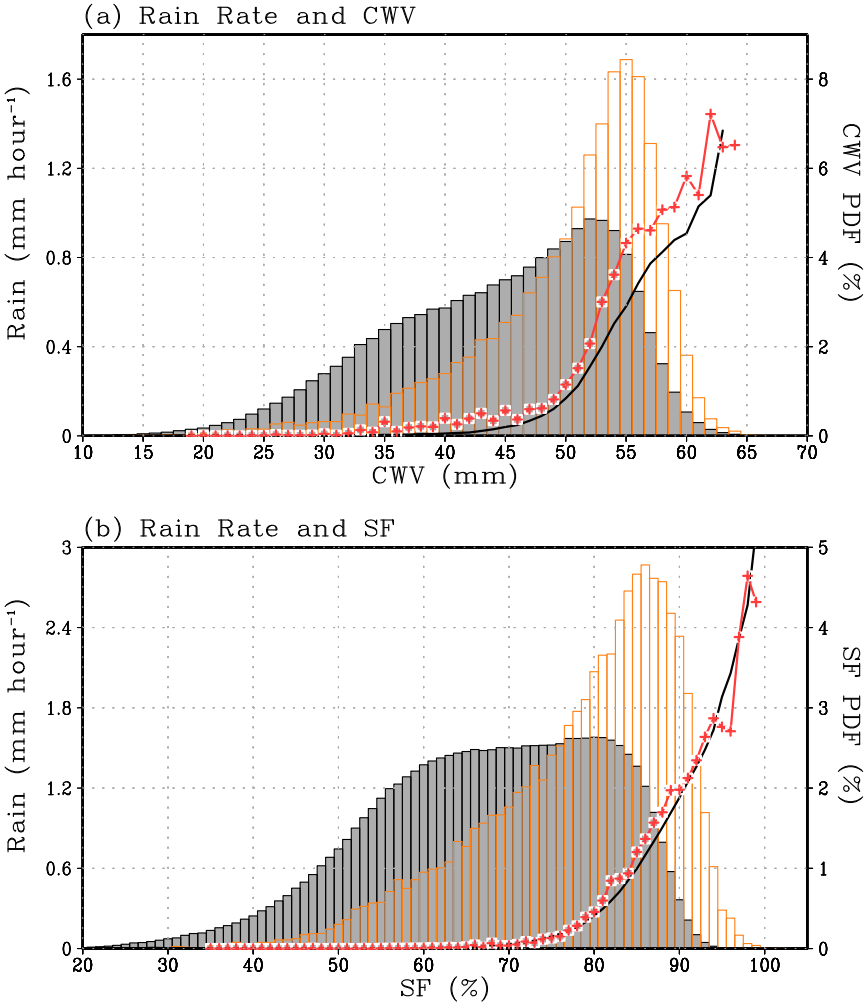

FIG. 4. (a) Rain rate averaged in 1-mm bins of CWV for the tropical Atlantic (5°–20°N, 15°–100°W; black curve) and for the wave pouches (red curve; bins with a sample size less than 10 are not shown). (b) As in (a), except that rain rate is stratified by saturation fraction with 1%-wide bins. The histograms of CWV and SF are shown with the ordinate on the right (gray bars for the tropical North Atlantic and orange bars for the wave pouches).

averages in the tail region of the PDF. On the other hand, the decrease in precipitation rate with increasing SF around these points is consistent with the increasing precipitation accompanied by decreasing CWV (or SF) from −18 to −6 h (Fig. 3) and may be explained by the highly nonlinear relationship between precipitation and tropospheric moisture at short time scales (Raymond et al. 2007; Masunaga 2012). Previous studies have shown that CWV builds up prior to the precipitation peak and may peak before the maximum precipitation (Mapes et al. 2006; Masunaga 2012). Furthermore, the reduction in CWV at the outer-pouch region, or the contraction of the moist core (Fig. 3), is possibly due to the enhanced low-level inflow near the genesis time, which converges moisture from large radii toward the pouch center (Fritz and Wang 2014).

4. Summary and discussion

The SSM/I and SSMIS data along with ERA-Interim and a pouch-track dataset were used to examine the moisture and precipitation evolution during TC formation. A particular strength of the SSM/I and SSMIS data is the simultaneous retrievals of precipitation rate and column water vapor. The data are available for about three decades and are the best-available long-term observation to investigate the coevolution of precipitation and moisture during tropical cyclogenesis.

It was found that precipitation increases substantially within 24 h prior to genesis, which is in good agreement with previous studies based on numerical model simulations or field observations (Nolan 2007; Wang 2012). It was also found that high precipitation rate is concentrated near the pouch center. The axisymmetric balance theory (e.g., Eliassen 1951; Willoughby 1979) suggests that the strong latent heat release near the pouch center can effectively drive the secondary circulation and spin up the system-scale circulation (e.g., Montgomery et al. 2006; Wang 2012).

Similar to precipitation, the azimuthal-mean CWV also increases with a decreasing radius, indicating that the wave pouch is effective in retaining moisture and preventing lateral dry-air intrusion. The high CWV is in turn favorable for moist deep convection (Zipser 2003; Wang 2014). It was also found that CWV starts increasing about 42 h prior to genesis, preceding the substantial increase in precipitation. The moisture and precipitation evolutions are consistent with the two-stage conceptual model for TC formation developed by Wang (2014) based on a numerical model simulation, in which the gradual moisture preconditioning (stage 1) leads to an abrupt transition to sustained deep convection (stage 2).

We also examined the relationship between precipitation and tropospheric moisture for the developing waves and compared them with the tropical North Atlantic. When precipitation is stratified by CWV, there are large discrepancies in the ensemble-average precipitation between the tropical North Atlantic ensemble and the pouch ensemble. When stratified by SF, the two ensembles show a remarkable agreement: precipitation increases at the same exponential rate above the same critical point of SF in the two groups. This suggested that the empirical relationship between precipitation and SF derived from the general tropical oceans in previous studies (e.g., Raymond 2000; Neelin et al. 2009) is also valid for incipient tropical cyclones. The histograms of SF, however, suggest that convection in a developing tropical cyclone has a higher probability of occurrence near and above criticality. This can be attributed to the positive feedback between convection and the low-level moisture convergence, which counteracts the negative feedback of precipitation on water vapor and makes convection more sustainable. This suggests that convection in a self-sustaining tropical cyclone is likely in a quasi-equilibrium state with high precipitation rate and moderately high SF.

This study is based on the composite analyses of a large number of incipient tropical cyclones. The large sample size makes the construction of statistically continuous evolution possible. On the other hand, composite means average out small-scale and transient features, and the evolution of individual storms is undoubtedly less smooth. In addition, although the passive microwave retrievals are the best data available to examine the coevolution of precipitation and moisture, it should be cautioned that the moisture retrievals are less reliable in regions of heavy precipitation. Analyses of field data or cloud-resolving numerical model simulations will be helpful to further test some of the findings in this study. It would also be interesting to examine whether the link between the PDF of SF and the positive precipitation–moisture convergence feedback in tropical cyclones can be generalized for other organized convective systems.

Acknowledgments. The SSM/I–SSMIS data were downloaded from http://www.remss.com/missions/ssmi. This work was supported by NOAA Grant NA15NWS4680007 and NRL Grant N00173-15-1-G004. The authors thank Dr. Tim Dunkerton and Dr. Steve Nesbitt for stimulating discussions and Dr. David Raymond and two anonymous reviewers for the constrictive comments on an earlier version of the manuscript.

REFERENCES

Braun, S. A., 2010: Reevaluating the role of the Saharan air layer in Atlantic tropical cyclogenesis and evolution. *Mon. Wea. Rev.*, **138**, 2007–2037, doi:10.1175/2009MWR3135.1.

Bretherton, C. S., M. E. Peters, and L. E. Back, 2004: Relationships between water vapor path and precipitation over the tropical oceans. *J. Climate*, **17**, 1517–1528, doi:10.1175/1520-0442(2004)017<1517:RBWVPA>2.0.CO;2.

Davis, C. A., and D. A. Ahijevych, 2012: Mesoscale structural evolution of three tropical weather systems observed during PREDICT. *J. Atmos. Sci.*, **69**, 1284–1305, doi:10.1175/JAS-D-11-0225.1.

——, and ——, 2013: Thermodynamic environments of deep convection in Atlantic tropical disturbances. *J. Atmos. Sci.*, **70**, 1912–1928, doi:10.1175/JAS-D-12-0278.1.

Dunion, J. P., 2011: Rewriting the climatology of the tropical North Atlantic and Caribbean Sea atmosphere. *J. Climate*, **24**, 893–908, doi:10.1175/2010JCLI3496.1.

Dunkerton, T. J., M. T. Montgomery, and Z. Wang, 2009: Tropical cyclogenesis in a tropical wave critical layer: Easterly waves. *Atmos. Chem. Phys.*, **9**, 5587–5646, doi:10.5194/acp-9-5587-2009.

Eliassen, A., 1951: Slow thermally or frictionally controlled meridional circulation in a circular vortex. *Astrophys. Norv.*, **5**, 19–60.

Fang, J., and F. Zhang, 2010: Initial development and genesis of Hurricane Dolly (2008). *J. Atmos. Sci.*, **67**, 655–672, doi:10.1175/2009JAS3115.1.

Fritz, C., and Z. Wang, 2014: Water vapor budget in a developing tropical cyclone and its implication for tropical cyclone formation. *J. Atmos. Sci.*, **71**, 4321–4332, doi:10.1175/JAS-D-13-0378.1.

Hankes, I., Z. Wang, G. Zhang, and C. L. Fritz, 2015: Merger of African easterly waves and formation of Cape Verde storms. *Quart. J. Roy. Meteor. Soc.*, **141**, 1306–1319, doi:10.1002/qj.2439.

Lee, C.-S., K. K. Cheung, J. S. Hui, and R. L. Elsberry, 2008: Mesoscale features associated with tropical cyclone formations in

the western North Pacific. *Mon. Wea. Rev.*, **136**, 2006–2022, doi:10.1175/2007MWR2267.1.

Mapes, B. E., S. Tulich, J.-L. Lin, and P. Zuidema, 2006: The mesoscale convection life cycle: Building block or prototype for large-scale tropical waves? *Dyn. Atmos. Oceans*, **42**, 3–29, doi:10.1016/j.dynatmoce.2006.03.003.

——, R. Milliff, and J. Morzel, 2009: Composite life cycle of maritime tropical mesoscale convective systems in scatterometer and microwave satellite observations. *J. Atmos. Sci.*, **66**, 199–208, doi:10.1175/2008JAS2746.1.

Masunaga, H., 2012: Short-term versus climatological relationship between precipitation and tropospheric humidity. *J. Climate*, **25**, 7983–7990, doi:10.1175/JCLI-D-12-00037.1.

Montgomery, M. T., and R. K. Smith, 2010: Tropical-cyclone formation: Theory and idealized modelling. *Proc. Seventh Int. Workshop on Tropical Cyclones*, La Réunion, France, WMO, 2.1. [Available online at http://www.meteo.physik.uni-muenchen.de/~roger/Publications/IWTC-VII_topic_2.1.pdf.]

——, M. E. Nicholls, T. A. Cram, and A. B. Saunders, 2006: A vortical hot tower route to tropical cyclogenesis. *J. Atmos. Sci.*, **63**, 355–386, doi:10.1175/JAS3604.1.

——, Z. Wang, and T. J. Dunkerton, 2010: Coarse, intermediate and high resolution numerical simulations of the transition of a tropical wave critical layer to a tropical storm. *Atmos. Chem. Phys.*, **10**, 10 803–10 827, doi:10.5194/acp-10-10803-2010.

Neelin, J. D., O. Peters, and K. Hales, 2009: The transition to strong convection. *J. Atmos. Sci.*, **66**, 2367–2384, doi:10.1175/2009JAS2962.1.

Nolan, D. S., 2007: What is the trigger for tropical cyclogenesis? *Aust. Meteor. Mag.*, **56**, 241–266.

Peters, O., J. D. Neelin, and S. W. Nesbitt, 2009: Mesoscale convective systems and critical clusters. *J. Atmos. Sci.*, **66**, 2913–2924, doi:10.1175/2008JAS2761.1.

Raymond, D. J., 2000: Thermodynamic control of tropical rainfall. *Quart. J. Roy. Meteor. Soc.*, **126**, 889–898, doi:10.1002/qj.49712656406.

——, and C. López Carrillo, 2011: The vorticity budget of developing typhoon Nuri (2008). *Atmos. Chem. Phys.*, **11**, 147–163, doi:10.5194/acp-11-147-2011.

——, S. L. Sessions, and Ž. Fuchs, 2007: A theory for the spinup of tropical depressions. *Quart. J. Roy. Meteor. Soc.*, **133**, 1743–1754, doi:10.1002/qj.125.

Tory, K. J., and W. M. Frank, 2010: Tropical cyclone formation. *Global Perspectives on Tropical Cyclones*, 2nd ed. J. Chan and J. D. Kepert, Eds., World Scientific, 55–92.

Wang, Z., 2012: Thermodynamic aspects of tropical cyclone formation. *J. Atmos. Sci.*, **69**, 2433–2451, doi:10.1175/JAS-D-11-0298.1.

——, 2014: Role of cumulus congestus in tropical cyclone formation in a high-resolution numerical model simulation. *J. Atmos. Sci.*, **71**, 1681–1700, doi:10.1175/JAS-D-13-0257.1.

——, and I. Hankes, 2014: Characteristics of tropical easterly wave pouches during tropical cyclone formation. *Mon. Wea. Rev.*, **142**, 626–633, doi:10.1175/MWR-D-13-00267.1.

——, M. T. Montgomery, and T. J. Dunkerton, 2009: A dynamically-based method for forecasting tropical cyclogenesis location in the Atlantic sector using global model products. *Geophys. Res. Lett.*, **36**, L03801, doi:10.1029/2008GL035586.

——, ——, and ——, 2010a: Genesis of pre–Hurricane Felix (2007). Part I: The role of the easterly wave critical layer. *J. Atmos. Sci.*, **67**, 1711–1729, doi:10.1175/2009JAS3420.1.

——, ——, and ——, 2010b: Genesis of pre–Hurricane Felix (2007). Part II: Warm core formation, precipitation evolution, and predictability. *J. Atmos. Sci.*, **67**, 1730–1744, doi:10.1175/2010JAS3435.1.

Wentz, F. J., 2013: SSM/I version-7 calibration report. Remote Sensing Systems Tech. Rep. 011012, 46 pp. [Available online at http://images.remss.com/papers/rsstech/2012_011012_Wentz_Version-7_SSMI_Calibration.pdf.]

Willoughby, H. E., 1979: Forced secondary circulations in hurricanes. *J. Geophys. Res.*, **84**, 3173–3183, doi:10.1029/JC084iC06p03173.

Zehr, R. M., 1992: Tropical cyclogenesis in the western North Pacific. NOAA Tech. Rep. NESDIS 61, 181 pp.

Zipser, E. J., 2003: Some views on ''hot towers'' after 50 years of tropical field programs and two years of TRMM data. *Cloud Systems, Hurricanes, and the Tropical Rainfall Measuring Mission (TRMM), Meteor. Monogr.*, No. 51, Amer. Meteor. Soc., 49–58.